

Screening and antiscreening in fullerene-like cages: dipole-field amplification with ionic nanocages

Pier Luigi Silvestrelli^{1,*}, S. Subashchandrabose^{1,2},

Abdolvahab Seif¹, and Alberto Ambrosetti¹

1) *Dipartimento di Fisica e Astronomia,*

Università degli Studi di Padova, 35131 Padova, Italy and

2) *Centre for Research and Development,*

Department of Physics, PRIST Deemed University,

Thanjavur, Tamilnadu-613403, India

(Dated: October 12, 2022)

Abstract

The successful synthesis of endohedral complexes consisting of nanoscale carbon cages that can encapsulate small molecules has been a remarkable accomplishment since these systems are ideal models to investigate how confinement effects can induce changes in structural and electronic properties of encapsulated molecular species. We here investigate from first principles screening effects observed when small molecules, characterized by a finite electronic dipole moment, such as HF, LiF, NaCl, and H₂O, are encapsulated into different nanoscale cages: C₆₀, C₇₂, B₃₆N₃₆, Be₃₆O₃₆, Li₃₆F₃₆, Li₃₆Cl₃₆, Na₃₆F₃₆, Na₃₆Cl₃₆, and K₃₆Br₃₆. Binding energies and electronic properties, of these complexes have been computed. In particular, detailed analysis of the effective dipole moment of the complexes and of the electronic charge distribution suggests that screening effects crucially depend on the nature of the intramolecular bonds of the cage: screening is maximum in covalent-bond carbon nanocages, while it is reduced in partially-ionic nanocages B₃₆N₃₆ and Be₃₆O₃₆, being very small in the latter cage which turns out to be almost “electrically transparent”. Interestingly, in the case of the ionic-bond nanocages, an antiscreening effect is observed: in fact, due to the relative displacement of positive and negative ions, induced by the dipole moment of the encapsulated molecule, these cages act as dipole-field amplifiers. Our results open the way to the possibility of tuning the dipole moment of nanocages and of generating electrostatic fields at the nanoscale without the aid of external potentials. Moreover, we can expect some transferability of the observed screening effects also to nanotubes and 2D materials.

INTRODUCTION

Buckminsterfullerene (C_{60}) is a carbon nanostructured allotrope with a cage-like fused-ring structure (truncated icosahedron) made of 20 carbon hexagons and 12 carbon pentagons where each carbon atom has three bonds. Since its discovery[1] this complex has received intense study, also considering that, although C_{60} is the most stable and the most common naturally occurring fullerene, many other cage-like nanostructures have been obtained and can be hypothesized, by both considering different numbers of C atoms and also replacing carbons with other atoms. For instance, it has been natural to search for cages made by B and N atoms, since the B-N pair is isoelectronic with a pair of C atoms; however, a fullerene structure made by 60 B and N atoms is not optimal since the presence of pentagonal rings does not allow a complete alternate sequence of B and N atoms. Fullerene-like alternate B-N cages can be formed introducing isolated squares characterized by 4 B-N bonds with alternate B and N atoms. In particular, a structure made by 36 B and 36 N atoms ($B_{36}N_{36}$), with a relatively large energy gap between the highest molecular orbital (HOMO) and the lowest molecular orbital (LUMO), has been found to be energetically very stable, both in theoretical first-principles studies and experimental investigations (see ref. 2 and references therein).

Interestingly, by high-energy collisions of ionized fullerene species, harsh conditions of high temperature and pressure, electric arc, or by organic synthesis methods (“molecular surgery”), it is nowadays possible to produce C_{60} endohedral complexes with metal ions, noble gases, and small molecules, such as H_2 , N_2 , H_2O , and CH_4 (the first organic molecule to be encapsulated)[3–8]. Such recent achievements in the synthesis of endohedral fullerene complexes have stimulated many experimental and theoretical investigations since the cavity inside fullerenes provides a unique environment for the study of isolated atoms and molecules. Moreover, these systems represent ideal models to study how confinement effects can induce changes in structural and electronic properties of small molecular species and also provide a possible way to alter the properties of the otherwise rather inert fullerenes. In particular, Kurotobi and Murata developed a synthetic route to surgically insert a single water molecule into the most common fullerene C_{60} [6], a remarkable achievement considering that water under normal conditions prefers to exist in a hydrogen bond forming hydrophilic environment. The water molecule, with its relatively large dipole moment (1.9 D), is ex-

pected to polarize the symmetric non-polar C_{60} cage. However, the theoretical study of such polarization effects has given rise to a scientific controversy. In fact, while Kurotobi and Murata[6], and Bucher[9] estimated a surprisingly high value of the dipole moment of the $H_2O@C_{60}$ complex (a value similar to that of the isolated water molecule), other theoretical first-principles studies[10–12] indicate that the dipole moment of $H_2O@C_{60}$ is instead much lower (about 0.5 D) than that for the isolated water, thus suggesting that a substantial counteracting dipole moment is induced in the C_{60} cage, which considerably screens the electric field produced by the dipole moment of the encapsulated water molecule. The residual dipole moment of $H_2O@C_{60}$ is still significant, which could have interesting implications for possible applications of fullerenes.

In this work, by adopting independent theoretical approaches, we confirm our previous conclusions[12] about the pronounced screening of the dipole moment of a water molecule encapsulated into C_{60} and extend the study to the encapsulation of some linear diatomic molecules, characterized by a dipole moment comparable (HF) to or even much larger (LiF and NaCl) than that of water. We also investigate screening effects in other cage-like nanostructures, such as $B_{36}N_{36}$, $Be_{36}O_{36}$, C_{72} (a carbon fullerene with the same structure of $B_{36}N_{36}$), and the hypothetical ionic-bond cages (again with the same structure of $B_{36}N_{36}$) $Li_{36}F_{36}$, $Li_{36}Cl_{36}$, $Na_{36}F_{36}$, $Na_{36}Cl_{36}$, and $K_{36}Br_{36}$.

In Figs. 1-3 we show some of the investigated nanocages, namely C_{72} , $B_{36}N_{36}$, and $Li_{36}F_{36}$, characterized by *covalent*-bonds, *partially-ionic* bonds, and *predominantly-ionic* bond, respectively (the figures are also representative of the other considered systems). We also plot the electron charge distribution to highlight the different bonding character of the nanocages.

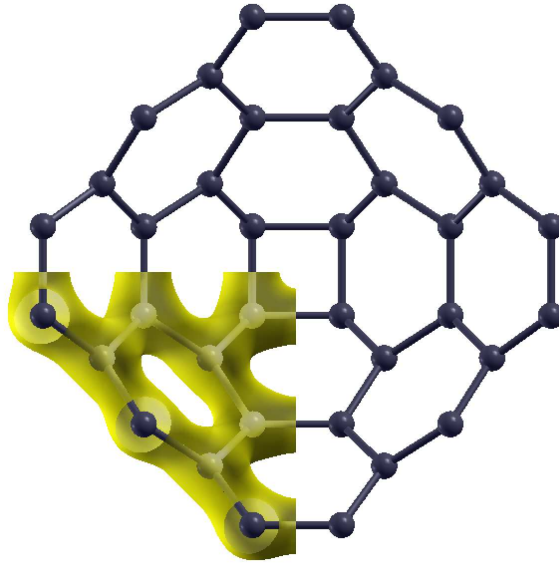


FIG. 1: C_{72} nanocage. The electron charge distribution corresponding to an isosurface of $1.0 e/\text{\AA}^3$ is also partially plotted (in a quarter of the figure).

Basically, our calculations of binding and electronic properties, and detailed analysis of the effective dipole moment of the complexes and the electronic charge distribution elucidate the encapsulation effects and suggest that the screening phenomenon crucially depends on the nature of the intramolecular bonds of the cage: screening is maximum in covalent-bond carbon nanocages, is reduced in partially-ionic ones, while in the case of the ionic-bond nanocages, an *antiscreening* effect is observed. Hence, the latter systems surprisingly act as dipole-field amplifiers.

METHODS

Our first-principles simulations have been performed with the Quantum-ESPRESSO *ab initio* package[13], within the framework of the Density Functional Theory (DFT). The investigated systems are located in periodically repeated cubic supercells, sufficiently large (finite-size effects have been carefully tested) to avoid significant spurious interactions due to periodic replicas: the lattice side ranges from 30 to 40 a.u., depending on the nanocage diameter. As a consequence, the sampling of the Brillouin Zone has been restricted to the Γ -point only. Electron-ion interactions were described using ultrasoft pseudopotentials and

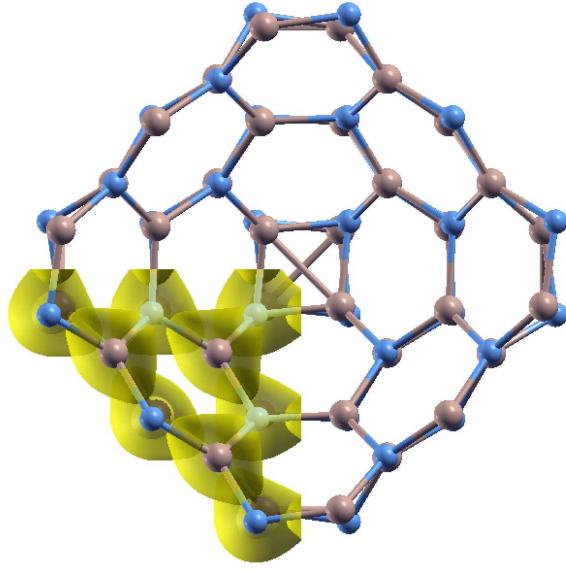


FIG. 2: B₃₆N₃₆ nanocage. Brown and blue balls represent B and N atoms, respectively. The electron charge distribution corresponding to an isosurface of $1.0 e/\text{\AA}^3$ is also partially plotted (in a quarter of the figure).

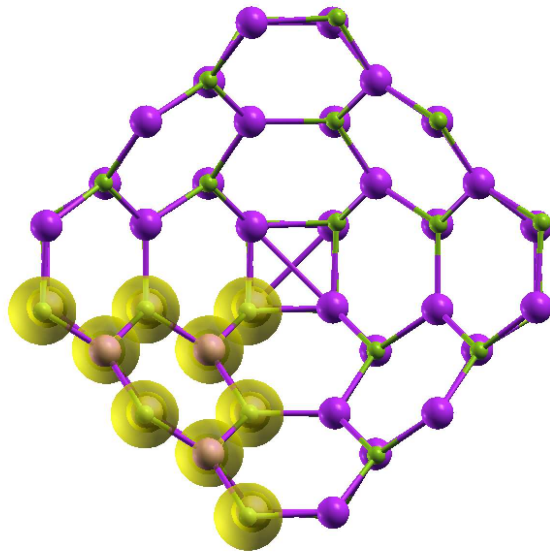


FIG. 3: Li₃₆F₃₆ nanocage. Violet and green balls represent Li and F atoms, respectively. The electron charge distribution corresponding to an isosurface of $1.0 e/\text{\AA}^3$ is also partially plotted (in a quarter of the figure).

the wavefunctions were expanded in a plane-wave basis set with an energy cutoff ranging from 34 to 80 Ry, depending on the atomic elements of the system. Since van der Waals (vdW) forces are expected to play an important role in the interaction of an encapsulated molecule with the surrounding cage[12], the calculations have been performed by adopting the rVV10 DFT functional[14] (this is the revised, more efficient version of the original VV10 scheme[15]), where vdW effects are included by introducing an explicitly nonlocal correlation functional. rVV10 has been found to perform well in many systems and phenomena where vdW effects are relevant, including several adsorption processes[14, 16, 17].

In order to corroborate the conclusions of our DFT-rVV10 calculations and better elucidate screening effects, we have also studied some of our systems by an alternative approach, namely the Self-Consistent Screening scheme (SCS)[18]. The SCS approach maps the dipole polarizability of the system into a set of coupled atom-centered Drude oscillators. The oscillators are parametrized according to the Tkatchenko-Scheffler[19] approach to account for charge hybridization. Moreover, SCS includes long-range many-body contributions up to infinite order, at an effective[20] Random Phase Approximation (RPA) level. In practice, one solves a discrete self-consistent electrostatic equation, that describes the coupled atomic polarizabilities in the presence of an external field. We also note that since SCS relies on atomic polarizabilities, it is a *linear* response theory by construction.

RESULTS

In Table I we report some basic properties of the cage-like nanostructures considered in the present study: the cage diameter, the cohesive energy, and the HOMO-LUMO energy gap E_g . For all the nanocages consisting of two different types of atoms E_g is considerable (ranging from 4.0 to 5.9 eV) and significantly larger than that of the carbon nanocages. The cohesive energy (per atom) is defined as:

$$E_c = (E - \sum_i^N E_i)/N, \quad (1)$$

where E is the total energy of the system, E_i is the energy of the isolated i -th atom, and N is the total number of atoms of the system. As can be seen, the cohesive energy is comparable for C_{60} , C_{72} , and $B_{36}N_{36}$, it is slightly smaller (in absolute value) for $Be_{36}O_{36}$, while it is considerably smaller for the ionic nanocages, although, for instance, E_c of $Li_{36}F_{36}$

is significantly larger than that of the Si_{60} cage, which was found to be structurally stable at room temperature; actually Si_{60} turns out to be stable towards spontaneous disintegration up to 700 K, according to previous first-principles simulations[21]. Also note that first-principles calculations showed the high stability of alkali-halide LiF nanotubes[22] and stable nanotube structures were also found for NaCl and KBr. E_c of the other considered ionic cages is instead smaller, so that we expect that these structures are less stable than $\text{Li}_{36}\text{F}_{36}$. In order to directly assess the stability of the $\text{Li}_{36}\text{F}_{36}$ nanocage we have carried out Molecular Dynamics (MD) simulations at different average temperatures. Newton's equations were integrated using the Verlet algorithm with a MD time step of 1.0 fs and typical total simulation times of 1 ps; the ionic temperature was set to the desired value by simple velocity rescaling. We observe that at $T=300$ K the $\text{Li}_{36}\text{F}_{36}$ structure is preserved, although some small distortions in the cage occur. According to our simulations, the $\text{Li}_{36}\text{F}_{36}$ nanocage disintegrates above 600 K, so that in principle this system could be indeed produced and experimentally observed at room temperature.

In Table I we also report the percent ionic character, which can be evaluated taking into account the electronegativities of the constituent atoms and using the Pauling's relation. As expected C_{60} , C_{72} , and Si_{60} are characterized by purely covalent bondings, $\text{Li}_{36}\text{F}_{36}$, $\text{Na}_{36}\text{F}_{36}$, $\text{Li}_{36}\text{Cl}_{36}$, $\text{Na}_{36}\text{Cl}_{36}$, and $\text{K}_{36}\text{Br}_{36}$ are systems with a predominant ionic character, while $\text{B}_{36}\text{N}_{36}$ and $\text{Be}_{36}\text{O}_{36}$ are partially ionic complexes (B is less electronegative than N and Be less electronegative than O). This aspect will be relevant for future considerations.

The electronic dipole moment of the systems is reported in Tables II-IV, and is computed as:

$$\mu = -e \int d\mathbf{r} \mathbf{r} n(\mathbf{r}) + \sum_i^N Z_i \mathbf{R}_i, \quad (2)$$

where $-e$ is the electron charge, $n(\mathbf{r})$ the electronic number density, and Z_i and \mathbf{R}_i are the valence and spatial coordinate of the i -th ion of the system, respectively. All the considered nanocages, in their optimized, isolated structure, are characterized by a negligible total dipole moment (in all cases not larger than 0.2 D). The scenario changes when a small molecule with a finite electronic dipole moment is encapsulated into the cages. We denote these endohedral complexes as X@Y , where $\text{X}=\text{HF}$, LiF , NaCl , and H_2O , while $\text{Y}=\text{C}_{60}$, C_{72} , $\text{B}_{36}\text{N}_{36}$, $\text{Be}_{36}\text{O}_{36}$, $\text{Li}_{36}\text{F}_{36}$, $\text{Na}_{36}\text{F}_{36}$, $\text{Li}_{36}\text{Cl}_{36}$, $\text{Na}_{36}\text{Cl}_{36}$, and $\text{K}_{36}\text{Br}_{36}$ (only the $\text{Na}_{36}\text{Cl}_{36}$

TABLE I: Diameter, cohesive energy E_c , HOMO-LUMO energy gap E_g , and percent ionic character of the bondings in the considered nanocages

system	diameter (Å)	E_c (eV)	E_g (eV)	ionic char.
C ₆₀	7.10	-7.92	1.65	0%
C ₇₂	8.58	-7.77	1.53	0%
B ₃₆ N ₃₆	8.70	-7.65	4.48	22%
Be ₃₆ O ₃₆	8.03	-6.09	4.89	58%
Li ₃₆ F ₃₆	9.36	-4.16	5.86	89%
Si ₆₀	11.67	-3.86	0.39	0%
Na ₃₆ F ₃₆	11.20	-3.53	4.79	90%
Li ₃₆ Cl ₃₆	11.30	-3.18	5.68	70%
Na ₃₆ Cl ₃₆	13.50	-2.77	4.73	71%
K ₃₆ Br ₃₆	18.50	-2.54	4.04	63%

and K₃₆Br₃₆ nanocages are sufficiently large to encapsulate a NaCl molecule without any significant distortion). When the small molecules are encapsulated into C₆₀ or C₇₂, as a consequence of the counteracting dipole moment induced in the cage, the effective dipole moment of the complex is severely reduced to a value that is less than 30% of the dipole moment of the isolated molecule. For H₂O@C₆₀ this confirms our previous findings[12] obtained computing the dipole moment using the Wannier-function approach[23] and agrees with experimental dielectric measurements performed at low temperature and infra-red spectra of H₂O@C₆₀ obtained at liquid Helium temperature, which measured a dipole moment of 0.5 ± 0.1 D[24, 25]. Our calculation is also consistent with the experimental estimate (0.45 ± 0.05 D) reported for HF@C₆₀[26] and with previous theoretical estimates for this system[27]. Therefore carbon fullerene cages shield more than 70% of the dipole moment of the encapsulated molecules and clearly act as molecular Faraday cages. With the B₃₆N₃₆ cage the screening effect is less pronounced, since the dipole moment reduction is about 40%, while in the case of Be₃₆O₃₆ this reduction amounts to only 10%, so that this cage turns out to be almost electrically “transparent” with X@Be₃₆O₃₆ that acquires essentially the same dipole moment of the encapsulated X molecule. A *qualitatively* different behavior occurs with en-

TABLE II: Electronic dipole moment μ of endohedral complexes with HF molecule inside; $\delta\mu$ denotes the change of the dipole moment of the endohedral complex with respect to that (1.78 D) of the encapsulated HF molecule when it is isolated. Binding energy (in square parenthesis using the PBE functional in place of rVV10) of endohedral complexes.

system	μ (D)	$\delta\mu$ (D)	E_{bind} (meV)
HF@C ₆₀	0.52	-1.26 (-71%)	-479 [-64]
HF@C ₇₂	0.47	-1.31 (-74%)	-617 [-61]
HF@B ₃₆ N ₃₆	1.09	-0.69 (-39%)	-374 [-63]
HF@Be ₃₆ O ₃₆	1.63	-0.15 (-8%)	-322 [-97]
HF@Li ₃₆ F ₃₆	2.13	+0.35 (+20%)	-100 [-59]
HF@Na ₃₆ F ₃₆	2.55	+0.77 (+43%)	-52 [-25]
HF@Li ₃₆ Cl ₃₆	2.21	+0.43 (+24%)	-74 [-17]
HF@Na ₃₆ Cl ₃₆	2.58	+0.80 (+45%)	-58 [-9]

capsulation into ionic nanocages: in fact an “anti-screening effect” is observed since the dipole moment of the endohedral complexes is significantly *increased*, by an amount ranging from 20 to 70%, thus indicating that ionic nanocages actually act as dipole-field amplifiers. Interestingly, the precise amount of percentage increase depends more on the specific ionic nanocage than on the dipole moment of the encapsulated molecule, even considering that LiF and NaCl are characterized by a value of the dipole moment much larger than that of HF or H₂O. In particular, ionic nanocages with Na and K atoms exhibit a more pronounced increase of the dipole moment than those with Li atoms. We have verified that the dipole moment of the different endohedral complexes does not change significantly by replacing the rVV10 DFT functional by the PBE one[28], that is a popular functional unable to properly take vdW interactions into account, thus showing that vdW effects are not relevant for this quantity which is evidently mostly determined by electrostatic interactions.

In order to better elucidate the mechanisms underlying the dipole-moment variations, a further analysis is performed. In Fig. 4 the changes in electron distribution, resulting from the encapsulation process are shown, for the HF@C₇₂ endohedral complex by plotting the *differential* charge density, $\Delta\rho$, defined as the difference between the total electron density

TABLE III: Electronic dipole moment μ of endohedral complexes with LiF and NaCl molecule inside; $\delta\mu$ denotes the change of the dipole moment of the endohedral complex with respect to those (6.17 D for LiF and 8.59 D for NaCl) of the encapsulated molecules when they are isolated. Binding energy (in square parenthesis using the PBE functional in place of rVV10) of endohedral complexes.

system	μ (D)	$\delta\mu$ (D)	E_{bind} (meV)
LiF@C ₆₀	1.73	-4.44 (-72%)	-1098 [-585]
LiF@C ₇₂	1.62	-4.55 (-74%)	-1088 [-538]
LiF@B ₃₆ NF ₃₆	3.80	-2.37 (-38%)	-958 [-541]
LiF@Be ₃₆ O ₃₆	5.52	-0.65 (-11%)	-877 [-569]
LiF@Li ₃₆ F ₃₆	7.98	+1.81 (+29%)	-402 [-314]
LiF@Na ₃₆ F ₃₆	7.99	+1.82 (+29%)	-215 [-175]
LiF@Li ₃₆ Cl ₃₆	7.55	+1.38 (+22%)	-225 [-150]
LiF@Na ₃₆ Cl ₃₆	8.63	+2.46 (+40%)	-158 [-95]
NaCl@Na ₃₆ Cl ₃₆	12.1	+3.51 (+41%)	-325 [-200]
NaCl@K ₃₆ Br ₃₆	14.9	+6.31 (+73%)	-170 [-110]

of the whole system and the superposition of the densities of the separated fragments (HF molecule and C₇₂ cage), keeping the same geometrical structure and atomic positions that these fragments have within the whole optimized system. This procedure is justified since, for non-ionic nanocages, the changes of atomic positions upon encapsulation of a small molecule are very small. Note that, in line with previous observations[27], the polar molecule HF is slightly displaced from the center of the nanocages, so that the H-cage distance is smaller than the F-cage one, due to the attractive electrostatic interactions between the H atom and the atoms of the cages. In Fig. 5 we also plot the one-dimensional profile $\Delta\rho(z)$, computed along the F-H z axis, as a function of z values, by integrating $\Delta\rho$ over the corresponding, orthogonal x, y planes. Inspection of these figures, that are representative of what happens in all the nanocages where a significant screening effect is observed, reveals that in HF@C₇₂ there is a pronounced electron charge accumulation in the region between the H atom and the cage with a charge depletion around the F atom, leading to the formation

TABLE IV: Electronic dipole moment μ of endohedral complexes with H₂O molecule inside; $\delta\mu$ denotes the change of the dipole moment of the endohedral complex with respect to that (1.86 D) of the encapsulated H₂O molecule when it is isolated. Binding energy (in square parenthesis using the PBE functional in place of rVV10) of endohedral complexes.

system	μ (D)	$\delta\mu$ (D)	E_{bind} (meV)
H ₂ O@C ₆₀	0.52	-1.34 (-72%)	-554 [+9]
H ₂ O@C ₇₂	0.52	-1.34 (-72%)	-531 [-25]
H ₂ O@B ₃₆ N ₃₆	1.17	-0.69 (-37%)	-547 [-84]
H ₂ O@Be ₃₆ O ₃₆	1.61	-0.25 (-13%)	-535 [-187]
H ₂ O@Li ₃₆ F ₃₆	2.20	+0.34 (+18%)	-152 [-76]
H ₂ O@Na ₃₆ F ₃₆	2.68	+0.82 (+44%)	-73 [-36]
H ₂ O@Li ₃₆ Cl ₃₆	2.32	+0.46 (+25%)	-87 [-25]
H ₂ O@Na ₃₆ Cl ₃₆	2.81	+0.95 (+51%)	-47 [-13]

of the counteracting dipole moment which considerably reduces the effective dipole moment of the endohedral complexes; clearly the overall response of these nanocages to the HF molecule dipole moment is a significant charge density shift. One can make quantitative the information contained in Fig. 5 by evaluating the induced dipole moment as:

$$\mu_{\text{ind}} = - \int dz z \Delta\rho(z) , \quad (3)$$

where $\Delta\rho(z)$ has been defined above. The numerical value of μ_{ind} is found to essentially coincide (see Fig. 5) with that of $\delta\mu$ reported in Table II for HF@C₇₂.

Instead, in predominantly ionic nano-cages, the dipole moment of the endohedral complexes is *increased* from the value of the isolated molecule that is encapsulated (*anti-screening effect*) and this dipole amplifications is mostly due to a slight cage distortion: in fact positive ions (Li+, Na+, and K+) are displaced with respect to the negative ions (F-, Cl-, and Br-). We can quantify this effect by computing the distance between the position of the center of mass of the positive ions and that of the center of mass of the negative ions: this quantity ranges from 3.3×10^{-3} Å for HF@Li₃₆F₃₆ to 5.5×10^{-2} Å for NaCl@K₃₆Br₃₆. Basically, as a small molecule with a permanent dipole moment is encapsulated into a ionic nanocage

this reacts in such a way to displace the positive ions with respect to the negative ions along the direction of the molecule dipole moment. This cage distortion accounts for more than 80% of the observed increase of the dipole moment; the remaining increase is due to the electronic charge polarization, and the small change of the interatomic distance of the encapsulated diatomic molecule. The basic mechanism of dipole increase is illustrated in Fig. 6 for $\text{NaCl}@\text{Na}_{36}\text{Cl}_{36}$, where this effect is pronounced: as can be seen, the Na^+ ions of the $\text{Na}_{36}\text{Cl}_{36}$ nanocage undergo a significant positive displacement below the Cl atom of the encapsulated Na-Cl molecule, while the Cl^- ions undergo a negative displacement particularly above the Na atom of the molecule. Also in partially-ionic nanocages, $\text{B}_{36}\text{N}_{36}$ and $\text{Be}_{36}\text{O}_{36}$, upon encapsulation one can detect a relative displacement of the center of mass of the two kinds of atoms, however this displacement is much smaller (by one or two orders of magnitude) than that observed in predominantly ionic nano-cages, so that the more standard mechanism of screening prevails.

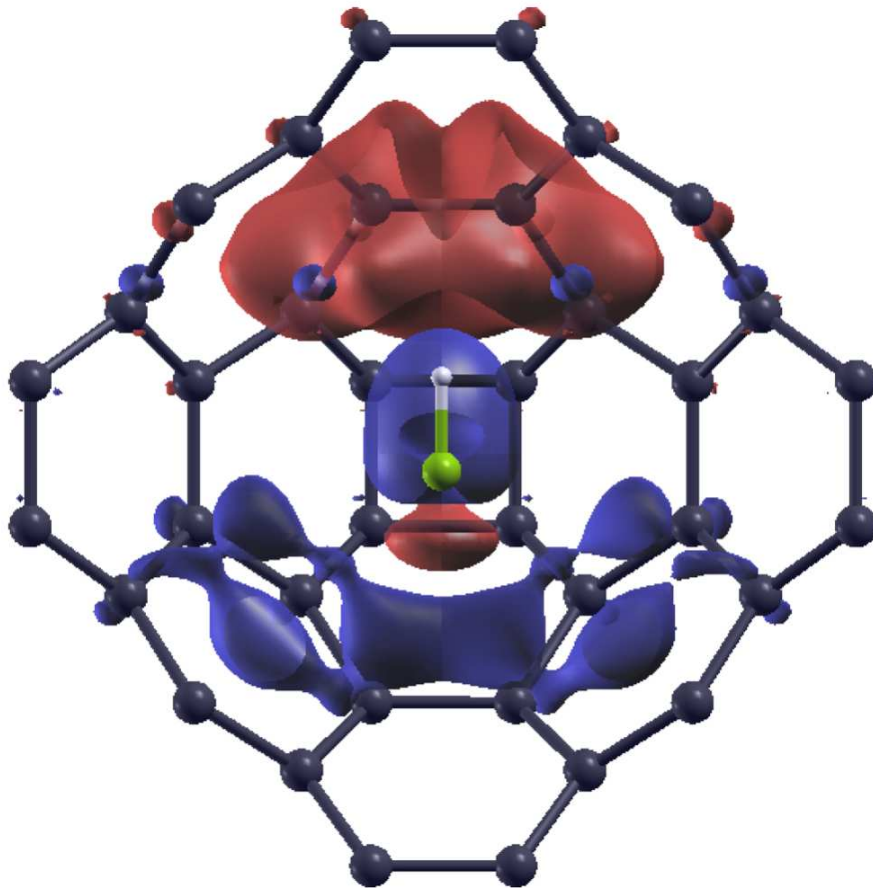


FIG. 4: Differential electron charge density, $\Delta\rho$, for $\text{HF}@C_{72}$, with isosurfaces shown at $\pm 2 \times 10^{-3} e/\text{\AA}^3$. Red areas indicate electron density gain, while blue areas indicate loss of electron density relative to the empty C_{72} cage and the isolated HF molecule.

In Table II we also report the binding energies of endohedral complexes; this is computed as the difference between the total energy of the $X@Y$ complex and the sum of the total energies of the constituent parts X and Y . We also add the binding energies obtained by replacing the rVV10 DFT functional with the PBE one. As can be seen, all the molecules are found to form stable complexes with the considered nanocages (with the exception of $\text{H}_2\text{O}@C_{60}$ using the PBE functional); however, differently from what found for the dipole moment, a proper inclusion of vdW effects is here crucial since these account for the dominant part of the binding energy between the cage and the HF and H_2O molecules, and represent a significant contribution also for the binding with the LiF and NaCl molecules, where electrostatic and induction-polarization interactions are important, as shown by the fact

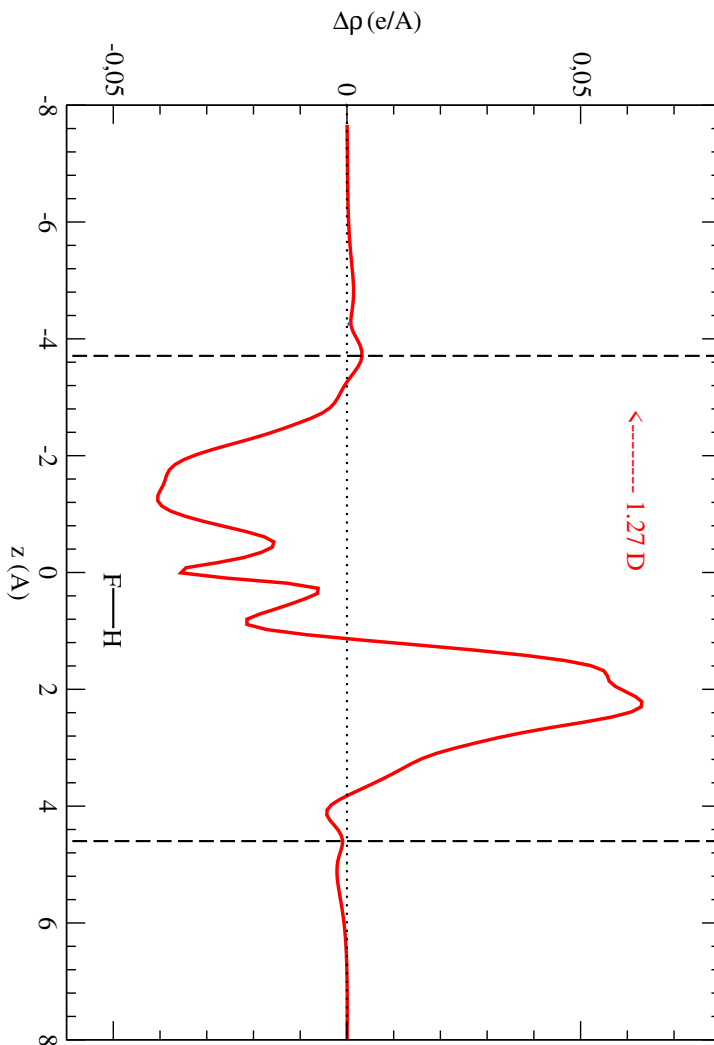


FIG. 5: Differential electron charge density, $\Delta\rho(z)$, along the F-H z axis, in HF@C₇₂. The vertical, black, dotted lines indicate the positions of the cage surface, while the red arrow represents the induced dipole moment with a numerical value obtained by integration on the z axis (see text).

that the binding energy predicted by the PBE functional is (in absolute value) not much smaller than that obtained by the vdW-corrected rVV10 functional. Note that in the present systems zero-point energy effects are expected to be small[27].

To complement the above first-principles DFT analysis, it is instructive to perform simplified SCS calculations for the dipole screening of a few relevant complexes. Within SCS the inner molecule is treated as a pointlike dipole, so that some information about the ac-

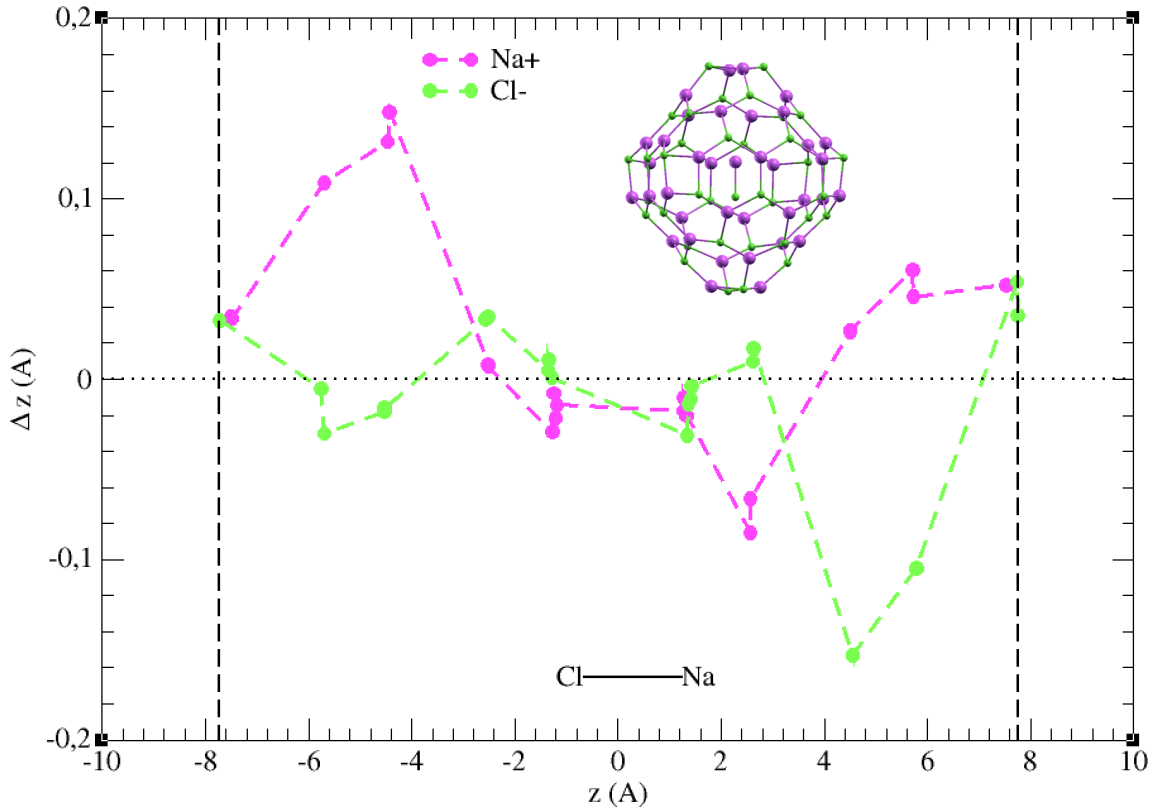


FIG. 6: $\text{NaCl}@_{\text{Na}_{36}\text{Cl}_{36}}$ complex: displacements, along the Cl-Na z axis, of Na^+ and Cl^- ions of the $\text{Na}_{36}\text{Cl}_{36}$ ionic nanocage upon encapsulation of NaCl : small circles represent the actual displacements of the ions, while the dashed lines are just a guide for the eye. The vertical, black, dotted lines indicate the positions of the cage surface.

tual molecule-fullerene interaction is lost. Moreover, given the linearity of the approach, screening is independent from the magnitude of the molecular dipole. We will thus consider encapsulated HF as the reference geometry, in order to extract qualitative trends. We note that the DFT dipole screening for C_{72} is qualitatively reproduced by SCS, reinforcing our previous conclusions: a reduction of the molecular dipole by 57% is found, although SCS cannot account for the quasi-metallic orbitals responsible for the charge localization observed in Fig. 4. In fact, while the charge of each Drude oscillator cannot move much from its initial position, the many-body coupling between all oscillators produces larger displacements where also DFT charge rearrangements are more concentrated. This result is compatible

with the long-ranged charge oscillations predicted in low-dimensional nanostructures [29] by a related Drude model: many-body couplings can strongly enhance the non-locality [30] of the density response in low dimensionality.

On the other hand, SCS, differently from what obtained by DFT, is found to roughly reproduce the same screening mechanism in all fullerene cages. For instance, the SCS screening is overestimated in $B_{36}N_{36}$, where a dipole reduction by 55% is found. Given the limitations of the naive Tkatchenko-Scheffler method in describing polar materials, we exploited here ionic polarizability data taken from ref.[31], as prescribed. Even more interesting, in $Li_{36}F_{36}$, no antiscreening is observed with SCS: the coupled atomic polarizabilities alone are clearly insufficient to cause dipole increase (in fact, even in this system SCS predicts a small screening of about 4%). This reconfirms that the leading antiscreening mechanism in ionic fullerenes is indeed played by the ionic rearrangements, that cannot be captured by SCS. We observe here the analogy with ionic crystals, where strong electron-phonon coupling can be associated to the rise of polarons [32], which involve a major interplay between charge localization and structural distortions.

CONCLUSIONS

We have presented the results of a first-principles study of screening effects in endohedral complexes made by small molecules, with a finite electronic dipole moment, encapsulated into different nanoscale cages. A detailed analysis of the effective dipole moment of the complexes and of the electronic charge distribution suggests that screening effects crucially depend on the nature of the intramolecular bonds of the cage: screening is maximum in covalent-bond carbon nanocages, while it is reduced in partially-ionic nanocages $B_{36}N_{36}$ and $Be_{36}O_{36}$, being very small in the latter cage which turns out to be almost “electrically transparent”. Interestingly, in the case of the ionic-bond nanocages, an *antiscreening* effect is observed: in fact, due to the relative displacement of positive and negative ions, induced by the dipole moment of the encapsulated molecule, these cages act as dipole-field amplifiers. Our results open the way to the possibility of tuning the dipole moment of nanocages and of generating electrostatic fields at the nanoscale without the aid of external potentials. Moreover, we can expect some transferability of the observed screening effects also to nanotubes and 2D materials.

ACKNOWLEDGEMENTS

We acknowledge funding from Fondazione Cariparo, Progetti di Eccellenza 2017, relative to the project “Engineering van der Waals Interactions: Innovative paradigm for the control of Nanoscale Phenomena”.

* pierluigi.silvestrelli@unipd.it

- [1] H. W. Kroto, J. R. Heath, S. C. O’Brien, R. F. Curl, R. E. Smalley, *Nature* **318**, 162 (1985).
”C₆₀: Buckminsterfullerene”
- [2] R. R. Zope, T. Baruah, M. R. Pederson, B. I. Dunlap, *Phys. Rev. A* **71**, 025201 (2005).
”Theoretical infra-red, Raman, and Optical spectra of the B₃₆N₃₆ cage”
- [3] T. Akasaka and S. Nagase, ”Endofullerenes: A New Family of Carbon Clusters”, Kluwer Academic, Dodrecht, Netherlands, 2002.
- [4] T. Suetsuna, N. Dragoe, W. Harneit, A. Weidinger, H. Shimotani, S. Ito, H. Takagi and K. Kitazawa, *Chem.–Eur. J.* **22**, 5079 (2002). ”Separation of N₂@C₆₀ and N@C₆₀”
- [5] K. Komatsu, M. Murata and Y. Murata, *Science* **307**, 238 (2005). ”Encapsulation of molecular hydrogen in fullerene C₆₀ by organic synthesis”
- [6] K. Kurotobi, Y. Murata, *Science* **333**, 613 (2011). ”A Single Molecule of Water Encapsulated in Fullerene C₆₀”
- [7] S. Bloodworth *et al.*, *Angew. Chem., Int. Ed.* **58**, 5038 (2019). ”First Synthesis and Characterization of CH₄@C₆₀”
- [8] A. Jaworski, N. Hedi, *Phys. Chem. Chem. Phys.* **23**, 21554 (2021). ”Local energy decomposition analysis and molecular properties of encapsulated methane in fullerene (CH₄@C₆₀)”
- [9] D. Bucher, *Chem. Phys. Lett.* **534**, 38 (2012). ”Orientational relaxation of water trapped inside C₆₀ fullerenes”
- [10] C. Ramachandran, N. Sathyamurthy, *Chem. Phys. Lett.* **410**, 348 (2005). ”Water clusters in a confined nonpolar environment”
- [11] K. Yagi, D. Watanabe, *Int. J. Quant. Chem.* **109**, 2080 (2009). ”Infrared spectra of water molecule encapsulated inside fullerene studied by instantaneous vibrational analysis”
- [12] B. Ensing, F. Costanzo, P. L. Silvestrelli, *J. Phys. Chem. A* **116**, 12184 (2012). ”On the

Polarity of Buckminsterfullerene with a Water Molecule Inside”

- [13] P. Giannozzi *et al.*, *J. Phys.: Condens. Matter* **21**, 395502 (2009). ”QUANTUM ESPRESSO: a modular and open-source software project for quantum simulations of materials”
- [14] R. Sabatini, T. Gorni, S. de Gironcoli, *Phys. Rev. B* **87**, 041108(R) (2013). ”Nonlocal van der Waals density functional made simple and efficient”
- [15] O. A. Vydrov, T. Van Voorhis, *J. Chem. Phys.* **133**, 244103 (2010). ”Nonlocal van der Waals density functional: The simpler the better”
- [16] P. L. Silvestrelli, A. Ambrosetti, *Phys. Rev. B* **91**, 195405 (2015). ”van der Waals corrected DFT simulation of adsorption processes on transition-metal surfaces: Xe and graphene on Ni(111)”
- [17] P. L. Silvestrelli, A. Ambrosetti, *J. Low. Temp. Phys.* **185**, 183 (2016). ”Van Der Waals-Corrected Density Functional Theory Simulation of Adsorption Processes on Noble-Metal Surfaces: Xe on Ag(111), Au(111), and Cu(111)”
- [18] A. Ambrosetti, A. M. Reilly, R. A. DiStasio Jr., A. Tkatchenko, *J. Chem. Phys.* **140**, 18A508 (2014). ”Long-range correlation energy calculated from coupled atomic response functions”
- [19] A. Tkatchenko, M. Scheffler, *Phys. Rev. Lett.* **102**, 073005 (2009). ”Accurate molecular van der Waals interactions from ground-state electron density and free-atom reference data”
- [20] A. Tkatchenko, A. Ambrosetti, R. A. DiStasio Jr., *Chem. Phys.* **138**, 074106 (2013). ”Interatomic methods for the dispersion energy derived from the adiabatic connection fluctuation-dissipation theorem”
- [21] Z. Chen, H. Jiao, G. Seifert, A. H. C. Horn, D. Yu, T. Clark, W. Thiel, P. von Ragué Schleyer, *J. Comput. Chem.* **24**, 948 (2003). ”The Structure and Stability of Si₆₀ and Ge₆₀ Cages: A Computational Study”
- [22] F. A. Fernandez-Lima, A. V. Henkes, E. F. da Silveira, M. A. Chaer Nascimento, *J. Phys. Chem. C* **116**, 4965 (2012). ”Alkali Halide Nanotubes: Structure and Stability”
- [23] N. Marzari and D. Vanderbilt, *Phys. Rev. B* **56**, 12847 (1997); P. L. Silvestrelli, N. Marzari, D. Vanderbilt, and M. Parrinello, *Solid St. Comm.* **107**, 7 (1998).
- [24] B. Meier, S. Mamone, M. Concistrè, J. Alonso-Valdesueiro, A. Krachmalnicoff, R. Whitby and M. Levitt, *Nat. Commun.* **6**, 8112 (2015). ”Electrical detection of ortho–para conversion in fullerene-encapsulated water”
- [25] A. Shugai *et al.*, *J. Chem. Phys.* **154**, 124311 (2021). ”Infrared spectroscopy of an endohedral

water in fullerene”

- [26] A. Krachmalnicoff *et al.*, Nat. Chem. **8**, 953 (2016). ”The dipolar endofullerene HF@C₆₀”
- [27] G. A. Dolgonos, G. H. Peslherbe, Phys. Chem. Chem. Phys. **16**, 26294 (2014). ”Encapsulation of diatomic molecules in fullerene C₆₀: implications for their main properties”
- [28] J. P. Perdew, K. Burke, and M. Ernzerhof, Phys. Rev. Lett. **77**, 3865 (1996). ”Generalized Gradient Approximation Made Simple”
- [29] A. Ambrosetti, N. Ferri, R. A. DiStasio Jr, A. Tkatchenko, Science **351**, 1171 (2016). ”Wavelike charge density fluctuations and van der Waals interactions at the nanoscale”
- [30] A. Ambrosetti, P.L. Silvestrelli, J. Phys. Chem. Lett. **10**, 2044 (2016). ”Faraday-like screening by two-dimensional nanomaterials: A scale-dependent tunable effect”
- [31] T. Gould, T. Bucko, J. Chem. Theory Comput. **12**, 3603 (2016). ”C₆ coefficients and dipole polarizability for all atoms and many ions in rows 1-6 of the periodic table”
- [32] J. Lafuente-Bartolome, C. Lian, W. H. Sio, I. G. Gurtubay, A. Eiguren, and F. Giustino, Phys. Rev. Lett. **129**, 076402 (2016). ”Unified Approach to Polarons and Phonon-Induced Band Structure Renormalization”